Tracking control of redundant manipulators with singularity-free orientation representation and null-space compliant behaviour

Fabio Vigoriti, Fabio Ruggiero, Vincenzo Lippiello, and Luigi Villani

Consorzio CREATE and PRISMA Lab,
Department of Electrical Engineering and Information Technology,
University of Naples, via Claudio 21, 80125, Naples, Italy
{fabio.vigoriti,fabio.ruggiero,vincenzo.lippiello,luigi.villani}@unina.it

Abstract. This paper presents a suitable solution to control the pose of the end-effector of a redundant robot along a pre-planned trajectory, while addressing an active compliant behaviour in the null-space. The orientation of the robot is expressed through a singularity-free representation form. To accomplish the task, no exteroceptive sensor is needed. While a rigorous stability proof confirms the developed theory, experimental results bolster the performance of the proposed approach.

Keywords: redundant robot tracking, null-space compliance, singularity-free orientation representation

1 Introduction

Over the last years, robotic systems are started to be used in those application areas where human-robot physical interaction becomes unavoidable and necessary. A new term, Socially Assistive Robotics (SAR), is defined in [6] for service robots working with humans. In certain cases, it might also be useful to measure, or at least estimate, the exchanged forces and to figure out whether the contact with the human operator has been unintentional or intentional (*i.e.*, required for collaborative tasks). The need of safety and dependability measures is discussed in [8] based on impact tests of a lightweight robot with a crash-test dummy for possible injuries that can happen in a SAR system, and on the severity of these injuries.

Hence, for safety reasons, a compliant behaviour is often requested to a robot. Such compliance can be in principle achieved through either a mechanical device or a suitable control law. In the former case, an elastic decoupling is placed between the actuators and the link, obtaining a fixed or a variable joint stiffness [1]. In the latter case, the compliant behaviour is obtained via software, like implementing an impedance control [7,9,19].

In the research project PHRIDOM, see [5], the components of a robotic application are discussed based on safety and dependability in physical human robot interaction. The mentioned components are mechanics, actuation control techniques and real-time planning for safety measures.

In the event of using a redundant robot, the compliant behaviour can be obtained both at the main task level [15,17] and in the null-space [18]. This last is helpful when the interaction control cannot interfere with the execution of the main task. In principle, the resulting external wrench affecting the main task should be properly measured or estimated: in this way, it is possible to design an impedance behaviour in the null-space without seizing the main one.

Using a redundant robot to minimize the injury possibilities prior to detect the contact is proposed in [13]. To this aim, a posture optimization technique is employed to make a redundant robot arm able to change its posture to minimize the impact forces along a given direction while carrying out the main task.

This paper extends what presented in [18], [20] by explicitly addressing the tracking case and employing a singularity-free representation for the orientation of the robot's end-effector, *e.g.*, axis-angle or unit quaternion. Notice that using one of these two orientation representations, the theoretical framework in [18] fails [1]. The sought aim is to control the robot arm while the end-effector has to follow a pre-planned trajectory in terms of both position and orientation, and the manipulator has to exhibit an active compliant behaviour in the null-space. A rigorous stability analysis is carried out thanks to the presence of a dynamic term in the controller, filtering both the effects of the velocity and of the external wrench, while no exteroceptive sensors are needed to fulfil the given task.

2 Mathematical framework

2.1 Notation

A redundant robot manipulator ($n > 6$) is considered in this paper, with n the number of joints. The vector $\boldsymbol{q} \in \mathbb{R}^n$ denotes the joint positions, while $\dot{\boldsymbol{q}} \in \mathbb{R}^n$ and $\ddot{\boldsymbol{q}} \in \mathbb{R}^n$ the joint velocities and accelerations, respectively.

Let Σ_i and Σ_e be the world inertial frame and the end-effector frame, respectively. The desired trajectory for Σ_e is specified in terms of the desired time-varying position $\boldsymbol{p}_d \in \mathbb{R}^3$, orientation $\boldsymbol{R}_d \in SO(3)$, linear velocity $\dot{\boldsymbol{p}}_d \in \mathbb{R}^3$, angular velocity $\boldsymbol{\omega}_d \in \mathbb{R}^3$, linear acceleration $\ddot{\boldsymbol{p}}_d \in \mathbb{R}^3$ and angular acceleration $\dot{\boldsymbol{\omega}}_d \in \mathbb{R}^3$, all expressed in Σ_i. On the other hand, $\boldsymbol{p}_e \in \mathbb{R}^3$ denotes the current position, $\dot{\boldsymbol{p}}_e \in \mathbb{R}^3$ the current linear velocity, $\boldsymbol{R}_e \in SO(3)$ the current orientation and $\boldsymbol{\omega}_e \in \mathbb{R}^3$ the current angular velocity of Σ_e with respect to Σ_i. The twist $\boldsymbol{v} = \left[\dot{\boldsymbol{p}}_e^{\mathrm{T}} \ \boldsymbol{\omega}_e^{\mathrm{T}}\right]^{\mathrm{T}} \in \mathbb{R}^6$ is used to compact notation. Finally, the identity and zero matrices are denoted by $\boldsymbol{I}_a \in \mathbb{R}^{a \times a}$ and $\boldsymbol{O}_a \in \mathbb{R}^{a \times a}$, respectively, while the zero vector is denoted by $\boldsymbol{0}_a \in \mathbb{R}^a$. With the given notation in mind, it is possible to define the so-called deviation matrix as $\widetilde{\boldsymbol{R}} = \boldsymbol{R}_d^{\mathrm{T}} \boldsymbol{R}_e \in SO(3)$. A non-minimal representation for $\widetilde{\boldsymbol{R}}$ can be obtained by resorting to 4 parameters $\boldsymbol{\alpha} \in \mathbb{R}^4$ [2,19].

[1] In detail, the proof of Proposition 3 within [18] cannot be applied whether the orientation error is chosen as it will be defined in this paper.

2.2 Axis-angle and unit quaternion

The matrix $\widetilde{\boldsymbol{R}}$ can be seen as a rotation of an angle $\widetilde{\phi} \in \mathbb{R}$ around the unit vector $\widetilde{\boldsymbol{r}} \in \mathbb{R}^3$. Such representation is not unique because $\widetilde{\boldsymbol{R}}(\widetilde{\phi}, \widetilde{\boldsymbol{r}}) = \widetilde{\boldsymbol{R}}(-\widetilde{\phi}, -\widetilde{\boldsymbol{r}})$. Expressing the columns of the current $\boldsymbol{n}_e$, $\boldsymbol{s}_e$, $\boldsymbol{a}_e \in \mathbb{R}^3$ and desired $\boldsymbol{n}_d$, $\boldsymbol{s}_d$, $\boldsymbol{a}_d \in \mathbb{R}^3$ rotation matrix of Σ_e with respect to Σ_i as $\boldsymbol{R}_e = \begin{bmatrix}\boldsymbol{n}_e & \boldsymbol{s}_e & \boldsymbol{a}_e\end{bmatrix}$ and $\boldsymbol{R}_d = \begin{bmatrix}\boldsymbol{n}_d & \boldsymbol{s}_d & \boldsymbol{a}_d\end{bmatrix}$, respectively, it is possible to choose the following compact expression for the orientation error [19]: $\widetilde{\boldsymbol{o}} = \frac{1}{2}\left(\boldsymbol{S}(\boldsymbol{n}_e)\,\boldsymbol{n}_d + \boldsymbol{S}(\boldsymbol{s}_e)\,\boldsymbol{s}_d + \boldsymbol{S}(\boldsymbol{a}_e)\,\boldsymbol{a}_d\right)$, where $\boldsymbol{S}(\cdot) \in \mathbb{R}^{3\times 3}$ is the skew-symmetric matrix. When the axes of $\boldsymbol{R}_d$ and $\boldsymbol{R}_e$ are aligned, $\widetilde{\boldsymbol{o}}$ is zero and $\widetilde{\boldsymbol{R}} = \boldsymbol{I}_3$. An equivalent expression for the orientation error in axis-angle representation is given by $\widetilde{\boldsymbol{o}} = \sin(\widetilde{\phi})\widetilde{\boldsymbol{r}}$ [2].

The ambiguity of the axis-angle representation can be overcome by introducing the *unit quaternion*. Define the quantities $\widetilde{\eta} = \cos\left(\widetilde{\phi}/2\right)$ and $\widetilde{\boldsymbol{\epsilon}} = \sin\left(\widetilde{\phi}/2\right)\widetilde{\boldsymbol{r}}$, where $\widetilde{\boldsymbol{\epsilon}} \in \mathbb{R}^3$ is the *vectorial part* of the quaternion, while $\widetilde{\eta} \in \mathbb{R}$ is its *scalar part*. The quaternion is referred to as unit since it satisfies $\widetilde{\boldsymbol{\epsilon}}^{\mathrm{T}}\widetilde{\boldsymbol{\epsilon}} + \widetilde{\eta}^2 = 1$, and it is a double cover of $SO(3)$ since it can be shown that $(\widetilde{\eta}, \widetilde{\boldsymbol{\epsilon}})$ and $(-\widetilde{\eta}, -\widetilde{\boldsymbol{\epsilon}})$ corresponds to the same rotation matrix. Therefore, $\widetilde{\boldsymbol{\epsilon}} = \boldsymbol{0}_3$ if and only if $\widetilde{\eta} = \pm 1$. This means that both $(\widetilde{\eta} = 1, \widetilde{\epsilon} = \boldsymbol{0}_3)$ and $(\widetilde{\eta} = -1, \widetilde{\boldsymbol{\epsilon}} = \boldsymbol{0}_3)$ correspond to $\widetilde{\boldsymbol{R}} = \boldsymbol{I}_3$, and thus $\boldsymbol{R}_e = \boldsymbol{R}_d$ as desired.

The orientation error for the axis-angle representation can be expressed in terms of unit quaternion as $\widetilde{\boldsymbol{o}} = 2\widetilde{\eta}\widetilde{\epsilon}$ [2]. In this paper the following orientation error definition is instead preferred $\widetilde{\boldsymbol{o}} = \widetilde{\boldsymbol{\epsilon}}$. It is possible to prove that, in case $\widetilde{\boldsymbol{o}} = \widetilde{\boldsymbol{\epsilon}} = \boldsymbol{0}_3$, the indetermination $\widetilde{\eta} = \pm 1$ does not affect the system stability [2]. Moreover, after deriving the kinematic equations for the unit quaternion as $\dot{\widetilde{\eta}} = (1/2)\widetilde{\boldsymbol{\epsilon}}^{\mathrm{T}}\widetilde{\boldsymbol{\omega}}$ and $\dot{\widetilde{\boldsymbol{\epsilon}}} = -(1/2)\left(\widetilde{\eta}\boldsymbol{I}_3 + \boldsymbol{S}(\widetilde{\boldsymbol{\epsilon}})\right)\widetilde{\boldsymbol{\omega}}$, set $\boldsymbol{\alpha} = \begin{bmatrix}\widetilde{\eta} & \widetilde{\boldsymbol{\epsilon}}^{\mathrm{T}}\end{bmatrix}^{\mathrm{T}}$, the time derivative of the orientation error can be written as

$$\dot{\widetilde{\boldsymbol{o}}} = \boldsymbol{L}_q(\boldsymbol{\alpha})\widetilde{\boldsymbol{\omega}}, \tag{1}$$

where $\widetilde{\boldsymbol{\omega}} = \boldsymbol{\omega}_d - \boldsymbol{\omega}_e \in \mathbb{R}^3$ is the angular velocity error and $\boldsymbol{L}_q(\boldsymbol{\alpha}) = -(1/2)\left(\widetilde{\eta}\boldsymbol{I}_3 + \boldsymbol{S}(\widetilde{\boldsymbol{\epsilon}})\right) \in \mathbb{R}^{3\times 3}$ is a nonsingular matrix.

2.3 Dynamics

The dynamic model of a robot arm in the joint space can be written as [19]

$$\boldsymbol{B}(\boldsymbol{q})\ddot{\boldsymbol{q}} + \boldsymbol{C}(\boldsymbol{q}, \dot{\boldsymbol{q}})\dot{\boldsymbol{q}} + \boldsymbol{g}(\boldsymbol{q}) = \boldsymbol{\tau} - \boldsymbol{\tau}_{ext}, \tag{2}$$

where $\boldsymbol{B}(\boldsymbol{q}) \in \mathbb{R}^{n\times n}$ is the inertia matrix in the joint space; $\boldsymbol{C}(\boldsymbol{q}, \dot{\boldsymbol{q}}) \in \mathbb{R}^{n\times n}$ is the so-called Coriolis matrix; $\boldsymbol{g}(\boldsymbol{q}) \in \mathbb{R}^n$ is the vector collecting gravity terms; $\boldsymbol{\tau} \in \mathbb{R}^n$ is the control torques vector; $\boldsymbol{\tau}_{ext} \in \mathbb{R}^n$ is the vector representing the effect of the resulting external wrench mapped on the joints. Since no force/torque sensors are employed, $\boldsymbol{\tau}_{ext}$ cannot be measured.

Denoting with $\boldsymbol{J}(\boldsymbol{q}) \in \mathbb{R}^{6\times n}$ the geometric Jacobian of the robot arm, the equation $\boldsymbol{\upsilon} = \boldsymbol{J}(\boldsymbol{q})\dot{\boldsymbol{q}}$, holds [19]. As an assumption, $\boldsymbol{J}(\boldsymbol{q})$ is always full rank[2]. Following the *joint space decomposition method* [15], it is possible to add $r = n - 6$

[2] Notice that, during the experiments, a damped least-squares solution is anyway employed.

auxiliary variables $\boldsymbol{\lambda} \in \mathbb{R}^r$ to the end-effector velocity $\boldsymbol{v}$ defined as $\dot{\boldsymbol{q}} = \boldsymbol{Z}(\boldsymbol{q})\boldsymbol{\lambda}$, where $\boldsymbol{Z}(\boldsymbol{q}) \in \mathbb{R}^{n \times r}$ is such that $\boldsymbol{J}(\boldsymbol{q})\boldsymbol{Z}(\boldsymbol{q}) = \boldsymbol{O}_{6 \times r}$. Notice that $\boldsymbol{Z}(\boldsymbol{q})$ spans the null-space of $\boldsymbol{J}(\boldsymbol{q})$. A convenient choice for $\boldsymbol{\lambda}$ is given by the left inertia-weighted generalized inverse of $\boldsymbol{Z}(\boldsymbol{q})$ [14], such that $\boldsymbol{\lambda} = \boldsymbol{Z}(\boldsymbol{q})^{\#}\dot{\boldsymbol{q}}$, with $\boldsymbol{Z}(\boldsymbol{q})^{\#} = \left(\boldsymbol{Z}(\boldsymbol{q})^{\mathrm{T}}\boldsymbol{B}(\boldsymbol{q})\boldsymbol{Z}(\boldsymbol{q})\right)^{-1}\boldsymbol{Z}(\boldsymbol{q})^{\mathrm{T}}\boldsymbol{B}(\boldsymbol{q})$. In the same way, it is possible to define a dynamically consistent generalized inverse Jacobian [12] as $\boldsymbol{J}(\boldsymbol{q})^{\#} = \boldsymbol{B}(\boldsymbol{q})^{-1}\boldsymbol{J}(\boldsymbol{q})^{\mathrm{T}}\left(\boldsymbol{J}(\boldsymbol{q})\boldsymbol{B}(\boldsymbol{q})^{-1}\boldsymbol{J}(\boldsymbol{q})^{\mathrm{T}}\right)^{-1}$ whose metrics is induced by the inertia matrix, as well as for $\boldsymbol{Z}(\boldsymbol{q})^{\#}$, and that plays a key role in null-space dynamics [15]. Therefore, the following decomposition for the joints velocity holds

$$\dot{\boldsymbol{q}} = \boldsymbol{J}(\boldsymbol{q})^{\#}\boldsymbol{v} + \boldsymbol{Z}(\boldsymbol{q})\boldsymbol{\lambda}, \tag{3}$$

Interested readers may find more details in [15,18].

3 Control design

The purpose of the control is to track a desired trajectory for the pose (position plus orientation) of the end-effector in the Cartesian space while fulfilling a compliant behaviour for the manipulator without interfering with the main task.

The first level of the designed controller is a classic inverse dynamics [19]

$$\boldsymbol{\tau} = \boldsymbol{B}(\boldsymbol{q})\boldsymbol{u}_q + \boldsymbol{C}(\boldsymbol{q}, \dot{\boldsymbol{q}})\dot{\boldsymbol{q}} + \boldsymbol{g}(\boldsymbol{q}), \tag{4}$$

where $\boldsymbol{u}_q \in \mathbb{R}^n$ is a new virtual control input. Replacing (4) into (2) yields the following closed-loop dynamics

$$\ddot{\boldsymbol{q}} = \boldsymbol{u}_q - \boldsymbol{B}(\boldsymbol{q})^{-1}\boldsymbol{\tau}_{ext}. \tag{5}$$

The following command acceleration can be thus designed [18]

$$\boldsymbol{u}_q = \boldsymbol{J}(\boldsymbol{q})^{\#}\left(\boldsymbol{u}_v - \dot{\boldsymbol{J}}(\boldsymbol{q})\dot{\boldsymbol{q}}\right) + \boldsymbol{Z}(\boldsymbol{q})\left(\boldsymbol{u}_\lambda - \dot{\boldsymbol{Z}}(\boldsymbol{q})^{\#}\dot{\boldsymbol{q}}\right), \tag{6}$$

where $\boldsymbol{u}_v \in \mathbb{R}^6$ and $\boldsymbol{u}_\lambda \in \mathbb{R}^r$ are new virtual control inputs in the Cartesian and in the null-space, respectively. The closed-loop dynamics can be projected in both spaces by substituting (6) into (5). Afterwards, multiplying both sides of the resulting equation by $\boldsymbol{J}(\boldsymbol{q})$ and $\boldsymbol{Z}(\boldsymbol{q})^{\#}$, respectively, yields

$$\dot{\boldsymbol{v}} = \boldsymbol{u}_v - \boldsymbol{J}(\boldsymbol{q})\boldsymbol{B}(\boldsymbol{q})^{-1}\boldsymbol{\tau}_{ext}, \tag{7}$$

$$\dot{\boldsymbol{\lambda}} = \boldsymbol{u}_\lambda - \boldsymbol{Z}(\boldsymbol{q})^{\#}\boldsymbol{B}(\boldsymbol{q})^{-1}\boldsymbol{\tau}_{ext}. \tag{8}$$

The design of $\boldsymbol{u}_v$ and $\boldsymbol{u}_\lambda$ is addressed in the following.

3.1 Design of $\boldsymbol{u}_v$

Let $\widetilde{\boldsymbol{p}} = \boldsymbol{p}_d - \boldsymbol{p}_e \in \mathbb{R}^3$ and $\dot{\widetilde{\boldsymbol{p}}} = \dot{\boldsymbol{p}}_d - \dot{\boldsymbol{p}}_e \in \mathbb{R}^3$ be the position and the linear velocity error vectors, respectively. Moreover, set $\dot{\boldsymbol{v}}_d = \left[\ddot{\boldsymbol{p}}_d^{\mathrm{T}}\ \dot{\boldsymbol{\omega}}_d^{\mathrm{T}}\right]^{\mathrm{T}} \in \mathbb{R}^6$, $\boldsymbol{e}_v =$

$\left[\dot{\widetilde{\boldsymbol{p}}}^{\mathrm{T}}\ \widetilde{\boldsymbol{\omega}}^{\mathrm{T}}\right]^{\mathrm{T}} \in \mathbb{R}^6$, and $\boldsymbol{e}_t = \left[\widetilde{\boldsymbol{p}}^{\mathrm{T}}\ \widetilde{\boldsymbol{o}}^{\mathrm{T}}\right]^{\mathrm{T}} \in \mathbb{R}^6$. Then, the input term $\boldsymbol{u}_v$ in the Cartesian space can be designed as

$$\boldsymbol{u}_v = \dot{\boldsymbol{v}}_d + \boldsymbol{D}_v \boldsymbol{e}_v + \boldsymbol{K}_v \boldsymbol{e}_t - \boldsymbol{J}(\boldsymbol{q})\boldsymbol{B}(\boldsymbol{q})^{-1}\boldsymbol{\gamma}, \tag{9}$$

with $\boldsymbol{K}_v = \mathrm{diag}(\boldsymbol{K}_p, \boldsymbol{K}_o) \in \mathbb{R}^{6\times 6}$, where $\boldsymbol{K}_p \in \mathbb{R}^{3\times 3}$ is a positive definite diagonal gain matrix and $\boldsymbol{K}_o \in \mathbb{R}^{3\times 3}$ is an invertible matrix, $\boldsymbol{D}_v \in \mathbb{R}^{6\times 6}$ a positive definite diagonal gain matrix, and the vector $\boldsymbol{\gamma} \in \mathbb{R}^n$ is defined such that its time derivative is equal to

$$\dot{\boldsymbol{\gamma}} = -\boldsymbol{K}_I(\boldsymbol{\gamma} + \boldsymbol{\tau}_{ext}) - \boldsymbol{K}_\gamma^{-1}\boldsymbol{B}(\boldsymbol{q})^{-1}\boldsymbol{J}(\boldsymbol{q})^{\mathrm{T}}\boldsymbol{e}_v, \tag{10}$$

where $\boldsymbol{K}_I \in \mathbb{R}^{n\times n}$ and $\boldsymbol{K}_\gamma \in \mathbb{R}^{n\times n}$ are positive definite diagonal gain matrices.

Examining (10) it is possible to notice that a measurement of $\boldsymbol{\tau}_{ext}$ is needed. Nonetheless, it is possible to show that (10) has a closed-form solution

$$\begin{aligned}\boldsymbol{\gamma}(t) = \boldsymbol{K}_I &\left(\boldsymbol{B}(\boldsymbol{q})\dot{\boldsymbol{q}} - \int_0^t \left(\boldsymbol{\tau} + \boldsymbol{C}(\boldsymbol{q},\dot{\boldsymbol{q}})^{\mathrm{T}}\dot{\boldsymbol{q}} - \boldsymbol{g}(\boldsymbol{q}) + \boldsymbol{\gamma}(\sigma)\right)\mathrm{d}\sigma\right) \\ &- \boldsymbol{K}_\gamma^{-1}\int_0^t \boldsymbol{B}(\boldsymbol{q})^{-1}\boldsymbol{J}(\boldsymbol{q})^{\mathrm{T}}\boldsymbol{e}_v \mathrm{d}\sigma,\end{aligned} \tag{11}$$

that can be directly replaced in (9). Notice that the measurements of neither $\ddot{\boldsymbol{q}}$ nor $\boldsymbol{\tau}_{ext}$ are required in (11). The first part of (11) is equal to the momentum-based observer introduced in [3]. The last part has been instead added to cope with the employed singularity-free orientation representations.

By substituting the designed control law (9) into (7), it is straightforward to write down the corresponding Cartesian space closed-loop equation as

$$\dot{\boldsymbol{e}}_v + \boldsymbol{D}_v \boldsymbol{e}_v + \boldsymbol{K}_v \boldsymbol{e}_t = \boldsymbol{J}(\boldsymbol{q})\boldsymbol{B}(\boldsymbol{q})^{-1}\boldsymbol{e}_\gamma, \tag{12}$$

where $\boldsymbol{e}_\gamma = \boldsymbol{\gamma} + \boldsymbol{\tau}_{ext} \in \mathbb{R}^n$.

3.2 Design of $\boldsymbol{u}_{\boldsymbol{\lambda}}$

Let $\boldsymbol{\lambda}_d \in \mathbb{R}^r$ and $\dot{\boldsymbol{\lambda}}_d \in \mathbb{R}^r$ be the null-space desired velocity and acceleration vectors, respectively. Define with $\boldsymbol{q}_d \in \mathbb{R}^n$ the time-varying desired value of the joint positions. This should be planned accordingly to ($\boldsymbol{p}_d$,$\boldsymbol{R}_d$) through the robot inverse kinematics. Moreover, let $\boldsymbol{e}_\lambda = \boldsymbol{\lambda}_d - \boldsymbol{\lambda} \in \mathbb{R}^r$ and $\boldsymbol{e}_q = \boldsymbol{q}_d - \boldsymbol{q} \in \mathbb{R}^n$ be the null-space velocity and the joint configuration errors, respectively. As highlighted in [4], $\boldsymbol{\lambda}$ is not integrable and it is not thus possible to define a position error in the null-space. Therefore, the design of $\boldsymbol{u}_\lambda$ follows [16,18] as

$$\boldsymbol{u}_\lambda = \dot{\boldsymbol{\lambda}}_d + \boldsymbol{\Lambda}_\lambda(\boldsymbol{q})^{-1}\left(\left(\boldsymbol{\mu}_\lambda(\boldsymbol{q},\dot{\boldsymbol{q}}) + \boldsymbol{D}_\lambda\right)\boldsymbol{e}_\lambda + \boldsymbol{Z}(\boldsymbol{q})^{\mathrm{T}}\left(\boldsymbol{K}_q\boldsymbol{e}_q + \boldsymbol{D}_q\dot{\boldsymbol{e}}_q\right)\right), \tag{13}$$

where $\boldsymbol{K}_q \in \mathbb{R}^{n\times n}$ and $\boldsymbol{D}_q \in \mathbb{R}^{n\times n}$ are definite positive gain matrices, $\boldsymbol{\Lambda}_\lambda(\boldsymbol{q}) = \boldsymbol{Z}(\boldsymbol{q})^{\mathrm{T}}\boldsymbol{B}(\boldsymbol{q})\boldsymbol{Z}(\boldsymbol{q}) \in \mathbb{R}^{r\times r}$, and $\boldsymbol{\mu}_\lambda(\boldsymbol{q},\dot{\boldsymbol{q}}) = \left(\boldsymbol{Z}(\boldsymbol{q})^{\mathrm{T}}\boldsymbol{C}(\boldsymbol{q},\dot{\boldsymbol{q}}) - \boldsymbol{\Lambda}_\lambda(\boldsymbol{q})\dot{\boldsymbol{Z}}(\boldsymbol{q})^{\#}\right)\boldsymbol{Z}(\boldsymbol{q}) \in$

$\mathbb{R}^{r\times r}$. Notice that $\boldsymbol{\Lambda}_\lambda(\boldsymbol{q})$ is positive definite, while $\dot{\boldsymbol{\Lambda}}_\lambda(\boldsymbol{q}) - 2\boldsymbol{\mu}_\lambda(\boldsymbol{q},\dot{\boldsymbol{q}})$ is skew-symmetric [18]. By substituting (13) into (8), it is possible to write down the null-space closed-loop equation as

$$\boldsymbol{\Lambda}_\lambda(\boldsymbol{q})\dot{\boldsymbol{e}}_\lambda + (\boldsymbol{\mu}_\lambda(\boldsymbol{q},\dot{\boldsymbol{q}}) + \boldsymbol{D}_\lambda)\,\boldsymbol{e}_\lambda + \boldsymbol{Z}(\boldsymbol{q})^{\mathrm{T}}\,(\boldsymbol{K}_q\boldsymbol{e}_q + \boldsymbol{D}_q\dot{\boldsymbol{e}}_q) = \boldsymbol{Z}(\boldsymbol{q})^{\mathrm{T}}\boldsymbol{\tau}_{ext}. \quad (14)$$

This acts as an impedance controller against the projection $\boldsymbol{\tau}_{ext}$ in the null-space. The matrix $\boldsymbol{\Lambda}_\lambda(\boldsymbol{q})$ represents the inertia in the null-space, while $\boldsymbol{\mu}_\lambda(\boldsymbol{q},\dot{\boldsymbol{q}})$ the Coriolis matrix in the same space. These matrices cannot be modified, as instead $\boldsymbol{D}_\lambda$, $\boldsymbol{K}_q$ and $\boldsymbol{D}_q$ that can be tuned to specify the desired null-space behaviour.

4 Proof of stability

Recalling the designed control inputs (9), (11) and (13), and the resulting closed-loop system equations (12) and (14), to rigorously prove the stability of the system, the state $\boldsymbol{x} = (\boldsymbol{e}_q, \boldsymbol{e}_t, \boldsymbol{e}_\upsilon, \boldsymbol{e}_\gamma, \boldsymbol{e}_\lambda) \in \mathbb{R}^m$, with $m = 2n + r + 12$, has to asymptotically go to zero. Conditional stability [16] is the concept employed in the provided proof. Therefore, it is worth introducing the following theorem.

Theorem 1. *Let $\bar{\boldsymbol{x}} = \boldsymbol{0}_m$ be an equilibrium point of the system $\dot{\boldsymbol{x}} = \boldsymbol{f}(\boldsymbol{x})$, with $\boldsymbol{f}(\boldsymbol{x}) \in \mathbb{R}^m$. Then, $\bar{\boldsymbol{x}}$ is asymptotically stable if, in a neighbourhood Ω of $\bar{\boldsymbol{x}}$, there exists a function $V \in \mathcal{C}^1$ such that*

1. *$V(\boldsymbol{x}) \geq 0$ for all $\boldsymbol{x} \in \Omega$ and $V(\bar{\boldsymbol{x}}) = 0$;*
2. *$\dot{V}(\boldsymbol{x}) \leq 0$ for all $\boldsymbol{x} \in \Omega$;*
3. *on the largest positive invariant set $\mathcal{L} \subseteq \mathcal{Y} = \{\boldsymbol{x} \in \Omega : \dot{V}(\boldsymbol{x}) = 0\}$, the system is asymptotically stable.*

Proof. See [11]. □

The following proposition proves the stability of (12) and (14).

Proposition 1. *Let $\boldsymbol{K}_\upsilon$ be a block-diagonal invertible matrix, while let $\boldsymbol{D}_\upsilon, \boldsymbol{K}_I$, $\boldsymbol{K}_\gamma, \boldsymbol{K}_q, \boldsymbol{D}_q, \boldsymbol{D}_\lambda$ be diagonal and positive definite matrices. Assume that $\dot{\boldsymbol{\tau}}_{ext} = \boldsymbol{0}_n$ and $\boldsymbol{\lambda}_d = \boldsymbol{Z}(\boldsymbol{q})^{\#}\dot{\boldsymbol{q}}_d$. Then, considering a redundant robot arm whose dynamic model is given by (2), the control laws (4), (9), (11) and (13) are able to*

1. *bring the state $\boldsymbol{x} = (\boldsymbol{e}_q, \boldsymbol{e}_t, \boldsymbol{e}_\upsilon, \boldsymbol{e}_\gamma, \boldsymbol{e}_\lambda)$ asymptotically to zero if $\boldsymbol{\tau}_{ext} = \boldsymbol{0}_n$, and $\boldsymbol{q}_d$ is chosen as fitting the pose $(\boldsymbol{p}_d, \boldsymbol{R}_d)$ at each instant of time;*
2. *bring the state asymptotically to zero except $\boldsymbol{e}_q$ if $\boldsymbol{\tau}_{ext} \neq \boldsymbol{0}_n$ and/or $\boldsymbol{q}_d$ is chosen such that the manipulator end-effector is not in the pose $(\boldsymbol{p}_d, \boldsymbol{R}_d)$ at each instant of time. In this case $\boldsymbol{q}$ tends to $\boldsymbol{q}^\star \neq \boldsymbol{q}_d$, that belongs to the set of solutions locally minimizing the quadratic function $\|\boldsymbol{K}_q\boldsymbol{e}_q + \boldsymbol{D}_q\dot{\boldsymbol{e}}_q - \boldsymbol{\tau}_{ext}\|^2$.*

Proof. The proof is based on Theorem 1. Define the following scalar function in a neighbourhood Ω of the origin $\bar{\boldsymbol{x}} = \boldsymbol{0}_m$

$$V(\boldsymbol{e}_\upsilon, \boldsymbol{e}_t, \boldsymbol{e}_\gamma) = \frac{1}{2}\boldsymbol{e}_\upsilon^{\mathrm{T}}\boldsymbol{e}_\upsilon + \frac{1}{2}\boldsymbol{e}_t^{\mathrm{T}}\boldsymbol{K}_V\boldsymbol{e}_t + \frac{1}{2}\boldsymbol{e}_\gamma^{\mathrm{T}}\boldsymbol{K}_\gamma\boldsymbol{e}_\gamma + f_V(\boldsymbol{\alpha}), \quad (15)$$

where $\boldsymbol{K}_V = \text{diag}(\boldsymbol{K}_p, \boldsymbol{K}_{V,2}) \in \mathbb{R}^{6\times6}$, with $\boldsymbol{K}_{V,2} \in \mathbb{R}^{3\times3}$ a positive definite diagonal matrix, and $f_V(\boldsymbol{\alpha}) \in \mathbb{R} \geq 0$. This last function depends on the chosen orientation representation. In the case of interest with $\widetilde{\boldsymbol{o}} = \widetilde{\boldsymbol{\epsilon}}$, then $f_V = k_\epsilon(\widetilde{\eta} - 1)^2$, with $k_\epsilon > 0$. Notice that $V(\boldsymbol{0}_m) = 0$ and since $V(\boldsymbol{e}_\upsilon, \boldsymbol{e}_t, \boldsymbol{e}_\gamma)$ is not defined on all the state variables, it is only semi-definite in Ω. This satisfies the first point of the Theorem 1. It is useful to compute the time derivative of $\boldsymbol{e}_t$ that is equal to

$$\dot{\boldsymbol{e}}_t = \begin{bmatrix} \dot{\widetilde{\boldsymbol{p}}}^{\mathrm{T}} & \boldsymbol{f}_m(\boldsymbol{\alpha}, \widetilde{\boldsymbol{\omega}})^{\mathrm{T}} \end{bmatrix}^{\mathrm{T}}, \tag{16}$$

with $\boldsymbol{f}_m(\boldsymbol{\alpha}, \widetilde{\boldsymbol{\omega}})$ chosen on the base of the available representation for the orientation. Having in mind (1), it yields $\boldsymbol{f}_m(\boldsymbol{\alpha}, \widetilde{\boldsymbol{\omega}}) = \boldsymbol{L}_q(\boldsymbol{\alpha})\widetilde{\boldsymbol{\omega}}$. Moreover the assumption $\dot{\boldsymbol{\tau}}_{ext} = \boldsymbol{0}_n$ yields

$$\dot{\boldsymbol{e}}_\gamma = \dot{\boldsymbol{\gamma}}. \tag{17}$$

Therefore, choosing $\boldsymbol{K}_o = k_\epsilon \boldsymbol{I}_3$ and $\boldsymbol{K}_{V,2} = 2k_\epsilon \boldsymbol{I}_3$, taking into account (12), (16) and (17), deriving (15) with respect to time yields $\dot{V} = -\boldsymbol{e}_v^{\mathrm{T}} \boldsymbol{D}_\upsilon \boldsymbol{e}_\upsilon - \boldsymbol{e}_\gamma^{\mathrm{T}} \boldsymbol{K}_\gamma \boldsymbol{K}_I \boldsymbol{e}_\gamma$, which is negative semi-definite in Ω, satisfying the second point of Theorem 1.

Now the objective is to fulfil the third point of Theorem 1. Define the set $\mathcal{Y} = \{\boldsymbol{x} \in \Omega : \boldsymbol{e}_q, \boldsymbol{e}_t, \boldsymbol{e}_\upsilon = \boldsymbol{0}_6, \boldsymbol{e}_\gamma = \boldsymbol{0}_r, \boldsymbol{e}_\lambda\}$. Besides, define

$$V_{\mathcal{Y}} = \frac{1}{2}\boldsymbol{e}_\lambda^{\mathrm{T}} \boldsymbol{\Lambda}_\lambda(\boldsymbol{q}) \boldsymbol{e}_\lambda + \frac{1}{2}\boldsymbol{e}_t^{\mathrm{T}} \boldsymbol{e}_t + \frac{1}{2}\boldsymbol{e}_q^{\mathrm{T}} \boldsymbol{K}_q \boldsymbol{e}_q, \tag{18}$$

which it positive definite in $\mathcal{Y}$. In this set, since $\boldsymbol{e}_\upsilon = \boldsymbol{0}_6$ then $\boldsymbol{\upsilon}_d = \boldsymbol{\upsilon}$. Moreover, having in mind (12) and since $\boldsymbol{e}_\gamma = \boldsymbol{0}_r$ as well, this implies that $\boldsymbol{e}_t = \boldsymbol{0}_6$. Because $\dot{\boldsymbol{e}_q} = \boldsymbol{Z}\boldsymbol{e}_\lambda$ and considering (3), (14) and (16), the time derivative of (18) within $\mathcal{Y}$ is $\dot{V}_{\mathcal{Y}} = -\boldsymbol{e}_\lambda^{\mathrm{T}} \left(\boldsymbol{D}_\lambda + \boldsymbol{Z}^{\mathrm{T}} \boldsymbol{D}_q \boldsymbol{Z} \right) \boldsymbol{e}_\lambda + \boldsymbol{e}_\lambda^{\mathrm{T}} \boldsymbol{Z}(\boldsymbol{q})^{\mathrm{T}} \boldsymbol{\tau}_{ext}$.

Initially, consider the first point of Preposition 1. Since $\tau_{ext} = \boldsymbol{0}_n$ and $\boldsymbol{q}_d$ is chosen such that the manipulator end-effector is located at $(\boldsymbol{p}_d, \boldsymbol{R}_d)$ at each instant of time, then $\dot{V}_{\mathcal{Y}} < -\boldsymbol{\lambda}^{\mathrm{T}} \boldsymbol{D}_\lambda \boldsymbol{\lambda}$, which is negative semi-definite in $\mathcal{Y}$. Invoking the La Salles invariance principle and having in mind (14), it is straightforward to prove that $\boldsymbol{e}_q \to \boldsymbol{0}_n$. Hence, for the above considerations, the system is asymptotically stable on the largest invariant set $\mathcal{L} \subseteq \mathcal{Y}$. This satisfies the third and last point of Theorem 1, and thus proves the first point of Proposition 1.

Finally, consider the second point of Proposition 1. Since $\boldsymbol{\tau}_{ext} \neq \boldsymbol{0}_n$ and $\boldsymbol{q}_d$ is not chosen such that the end-effector is located at the desired configuration $(\boldsymbol{p}_d, \boldsymbol{R}_d)$ at each instant of time, all the states variables of $\boldsymbol{x}$ goes asymptotically to zero except $\boldsymbol{e}_q$. As a matter of fact $\boldsymbol{q} \to \boldsymbol{q}^\star$ as shown in [18]. This happens because the robot reaches a joints configuration $\boldsymbol{q}^\star$ compatible with the main task $(\boldsymbol{p}_d, \boldsymbol{R}_d)$ since $\boldsymbol{e}_t = \boldsymbol{0}_6$ and minimizing the elastic potential energy $\|\boldsymbol{K}_q \boldsymbol{e}_q + \boldsymbol{D}_q \dot{\boldsymbol{e}}_q - \boldsymbol{\tau}_{ext}\|^2$. The solution of such a minimization is found by solving $\boldsymbol{Z}(\boldsymbol{q})^{\mathrm{T}} \left(\boldsymbol{K}_q \boldsymbol{e}_q + \boldsymbol{D}_q \dot{\boldsymbol{e}}_q - \boldsymbol{\tau}_{ext} \right) = \boldsymbol{0}_r$. Subsequently, $\dot{V}_{\mathcal{Y}}$ is less or equal to $-\boldsymbol{\lambda}^{\mathrm{T}} \boldsymbol{D}_\lambda \boldsymbol{\lambda}$, and thus $\boldsymbol{e}_\lambda$ tends to zero: this proves the second point of Proposition 1. □

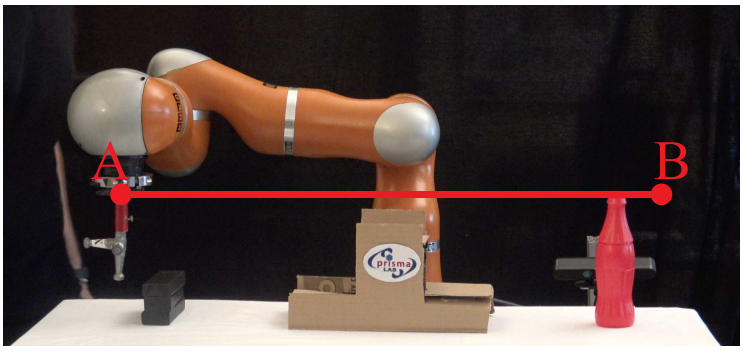

Fig. 1. The KUKA LWR4 employed for the experiments in the initial, and desired, configuration for the joints, and with the desired orientation for the end-effector.

5 Experiments

Experimental validation has been carried out on a KUKA LWR4 with $n = 7$. For each case study described below the controller sample time is equal to 2 ms, while the gains have been experimentally tuned to the following values: $\boldsymbol{K}_p = 150\boldsymbol{I}_2$, $\boldsymbol{K}_o = 150\boldsymbol{I}_3$, $\boldsymbol{D}_v = \text{blockdiag}\{20\boldsymbol{I}_2, 10\boldsymbol{I}_3\}$, $\boldsymbol{K}_I = 10\boldsymbol{I}_7$, $\boldsymbol{K}_\gamma = 100\boldsymbol{I}_7$, $\boldsymbol{K}_q = 5\boldsymbol{I}_7$, $\boldsymbol{D}_\lambda = 5\boldsymbol{I}_5$. The computation of $\boldsymbol{Z}(\boldsymbol{q})$ has been carried out in a symbolic way thanks to the Mathematica software. Without loss of generality, only the unit quaternion representation is employed in the following.

Three case studies are investigated. The considered scenario is depicted in Fig. 1. In the first case study the robot end-effector has to follow the path from A to B, whose length is about 0.6 m, keeping fixed the intial orientation. The timing law along the path is a trapezoidal acceleration with the cruise acceleration set to 0.15 m/s^2 [19]. By following the path, the tool attached to the end-effector crashes against the obstacles. However, since only the two planar positions variables in Σ_i and the orientation are constrained (the vertical position is left free), the dimension of $\boldsymbol{\lambda}$ is $r = 2$. This allows a human operator to push the robot to avoid obstacles by changing the configuration in the null space. It is worth pointing out that, due to the human presence, it is not possible to guarantee a constant $\boldsymbol{\tau}_{ext}$ during the experiments. Even if the developed theory shows asymptotic stability only for $\dot{\boldsymbol{\tau}}_{ext} = \boldsymbol{0}_n$, the overall performance remains good as admirable in the next subsections. The desired $\boldsymbol{q}_d$ is chosen off-line such that at each instant of time the end-effector is kept on the designed path.

In the second case study, the robot performs the same task, but $\boldsymbol{K}_q$ is set to zero. Hence, the robot does not come back to the planned $\boldsymbol{q}_d$ when pushed.

In the third case study, the two obstacles at the boundaries are removed: only the central obstacle depicted in Fig. 1 is kept. The matrix $\boldsymbol{K}_q$ is set back to its tuned value. The same position path is followed but the orientation has to follow a desired trajectory as well. The initial and final quaternions are $\boldsymbol{\alpha}_{init} = \begin{bmatrix}0.007 & 0.9336 & 0.3581 & -0.0007\end{bmatrix}^{\mathrm{T}}$ and $\boldsymbol{\alpha}_{fin} = \begin{bmatrix}0.7071 & 0.7071 & 0 & 0\end{bmatrix}^{\mathrm{T}}$. An angle-axis orientation planner is then built [19], with a trapezoidal acceleration whose cruise

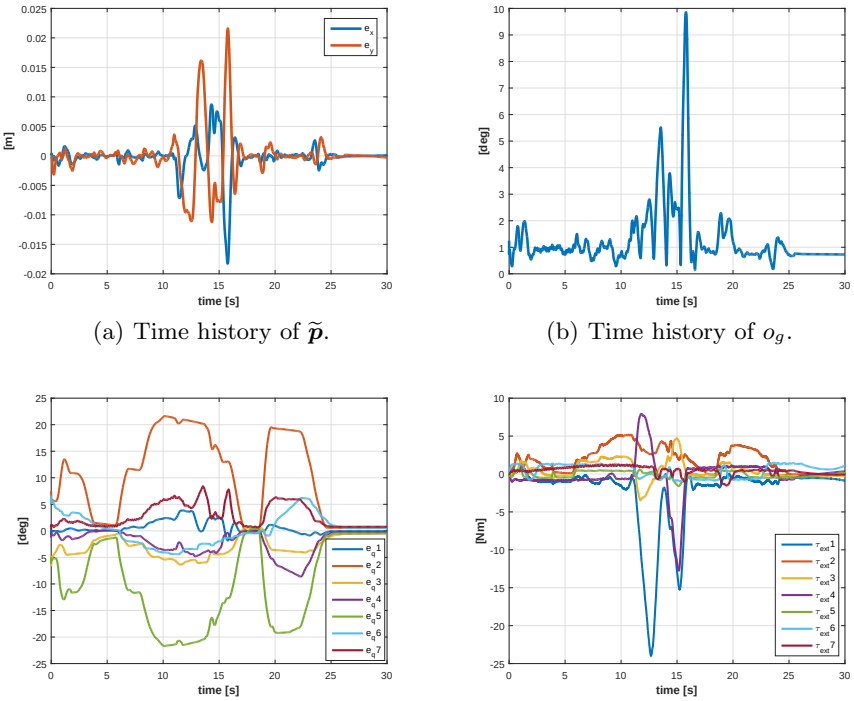

(a) Time history of $\widetilde{\boldsymbol{p}}$.

(b) Time history of o_g.

(c) Time history of $\boldsymbol{e}_q$.

(d) Time history of $\boldsymbol{\gamma}$.

Fig. 2. Time histories related to the first case study.

value is 0.15 rad/s^2. Again, the planned movement leads to a collision between the tool attached at the end-effector and the central obstacle. A human operator can reconfigure the robot internally by pushing it to avoid the object since the vertical position is not constrained. Again, the dimension of $\boldsymbol{\lambda}$ is $r = 2$.

5.1 Case Study 1

Time histories related to this first case study are depicted in Fig. 2. The two planar components of $\widetilde{\boldsymbol{p}}$ in Σ_i are shown in Fig. 2(a): the overall graph error is between ± 0.02 m, while its maximum is reached at about 15 s when there is a relevant interaction with the human operator, as it is also possible to check from Fig. 2(d) where the $\boldsymbol{\gamma}$ term, resembling $\boldsymbol{\tau}_{ext}$, is represented. From Fig. 2(d), it is also possible to see that human interaction happens at around 1 s, 6 s, 10 s, 15 s and 18 s to both avoid obstacles and test robustness.

The orientation error $\widetilde{\boldsymbol{o}}$ is depicted in Fig. 2(b) through its geodesic measure o_g in $SO(3)$ [10]. While the non-dimensional term $\widetilde{\boldsymbol{o}}$ is directly used in the control and it is not a clearly understandable for a reader, the geodesic measure is expressed in radians (or degree) and represents the distance of the deviation matrix $\widetilde{\boldsymbol{R}}$ from the identity. Expressing with $\|\cdot\|_F$ the Frobenius norm, the

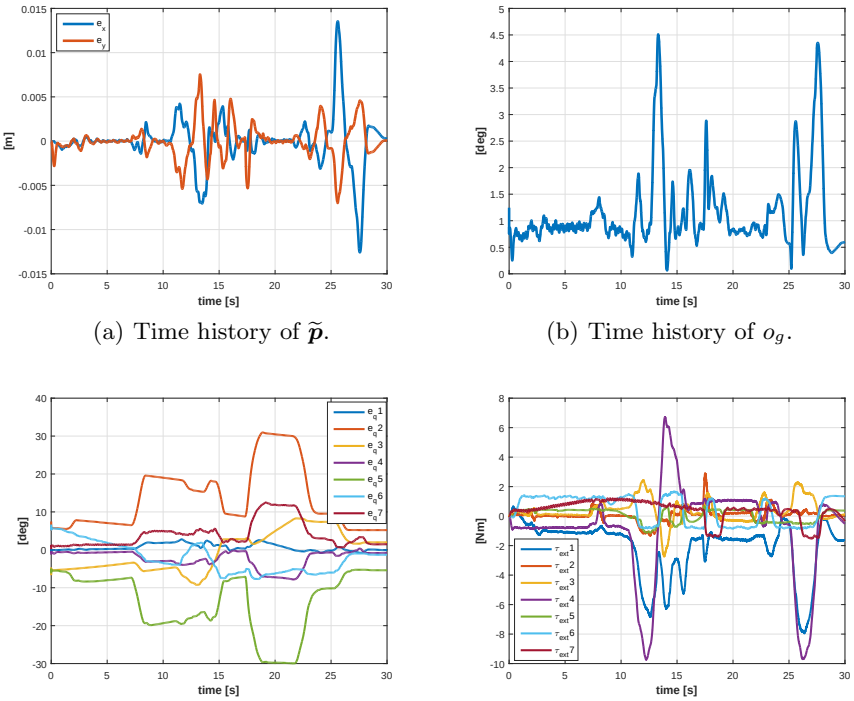

(a) Time history of $\widetilde{\boldsymbol{p}}$.

(b) Time history of o_g.

(c) Time history of $\boldsymbol{e}_q$.

(d) Time history of $\boldsymbol{\gamma}$.

Fig. 3. Time histories related to the second case study.

geodesic measure can be computed as $o_g = 1/\sqrt{2}\|\log\widetilde{\boldsymbol{R}}\|_F$. Within Section 2.2, and the references therein, it is possible to find the relations linking $\widetilde{\boldsymbol{R}}$ with $\widetilde{\boldsymbol{o}}$. From the time history related to the first case study, it is remarkable that the orientation error is under the 3 deg for most of time. The maximum error is reached again around 15 s. It is worth highlighting that the error does not come back exactly to zero due to the presence of non-negligible joint friction and other small uncertainties that the system is not able to recover.

Finally, the time history of $\boldsymbol{e}_q$ is depicted in Fig. 2(c). It is possible to appreciate that once the interaction with the human is ended, the manipulator tends to come back to the (time-varying) desired $\boldsymbol{q}_d$.

5.2 Case Study 2

The time histories related to this case study are depicted in Fig. 3. The position error $\widetilde{\boldsymbol{p}}$ is shown in Fig. 3(a) for the two planar components expressed in Σ_i: the overall graph error is between ± 0.015 m. Fig. 3(d) shows instead the time history of the $\boldsymbol{\gamma}$ term, in which it is possible to see that human interaction happens at around 2 s, 8 s, 11 s, 13 s, 17 s, 22 s and 26 s to both avoid obstacles and test robustness. The geodesic measure o_g related to $\widetilde{\boldsymbol{o}}$ is depicted in Fig. 2(b). Such

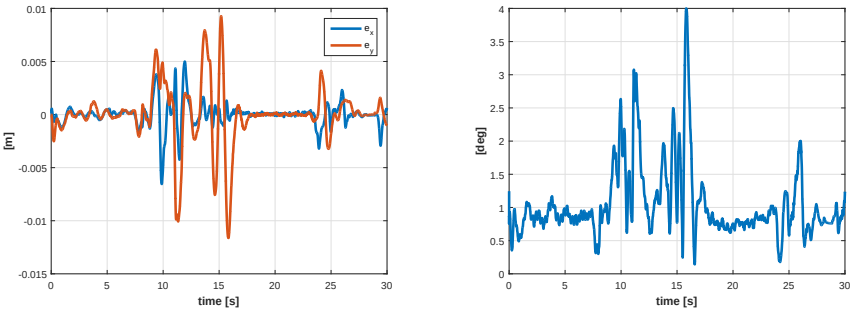

(a) Time history of $\widetilde{\boldsymbol{p}}$. (b) Time history of o_g.

Fig. 4. Time histories related to the third case study.

orientation error is lower than 2 deg for most of experiment. The maximum error is reached around 13 s and 26 s. Finally, the time history of $\boldsymbol{e}_q$ is depicted in Fig. 3(c). It is possible to appreciate that once the interaction with the human is ended, the manipulator stays in the reached internal configuration since the gain $\boldsymbol{K}_q$ has been set to zero. The manipulator behaviour is pretty similar to the one achievable through a direct zero-force control law.

5.3 Case Study 3

Time histories related to this case study are depicted in Fig. 4. The position error $\widetilde{\boldsymbol{p}}$ is shown in Fig. 4(a) for the two planar components expressed in Σ_i: the overall graph error is between ± 0.01 m. The geodesic measure o_g related to $\widetilde{\boldsymbol{o}}$ is depicted in Fig. 4(b). Such orientation error is lower than 3 deg for most of experiment. The maximum error of about 4 deg is reached around 16 s. The time histories for the $\boldsymbol{\gamma}$ term and $\boldsymbol{e}_q$ are not reported for brevity since they are very similar to the first case study, in which the end-effector desired behaviour was to track a path for the position and keep fixed the orientation. This last case study, instead, shows how the proposed controller is able to track the desired Cartesian pose, while preserving the possibility to act in the null-space with a compliance behaviour preserving the main task. These and other experiments, like pouring a water in a moving glass, are available in the related video-clip[3].

6 Conclusion

In this paper, a framework to control a redundant manipulator in the Cartesian space for a tracking task is designed addressing a singularity-free representation for the orientation, and allowing the possibility to change the null-space configuration of the manipulator without affecting the main task. The designed controller does not need any exteroceptive sensors to accomplish the task, as

[3] `https://www.youtube.com/watch?v=PirdFEAE_D8`

well as no joints torque sensors are requested. Theory and experimental results bolster the effectiveness of the proposed control scheme.

Acknowledgements

The research leading to these results has been supported by the RoDyMan project, which has received funding from the European Research Council FP7 Ideas under Advanced Grant agreement number 320992. The authors are solely responsible for the content of this manuscript.

References

1. Bicchi, A., Tonietti, G.: Fast and soft arm tactics: Dealing with the safety performance trade-off in robot arms design and control. IEEE Robotics and Automation Magazine 11(2), 22–33 (2004)
2. Caccavale, F., Natale, C., Siciliano, B., Villani, L.: Resolved-acceleration control of robot manipulators: A critical review with experiments. Robotica 16, 565–573 (1998)
3. De Luca, A., Albu-Schaffer, A., Haddadin, S., Hirzinger, G.: Collision detection and safe reaction with the DLR-III lightweight robot arm. In: 2006 IEEE/RSJ International Conference on Intelligent Robots Systems. pp. 1623–1630. Beijing, C (2006)
4. De Luca, A., Oriolo, G.: Nonholonomic behavior in redundant robots under kinematic control. IEEE Transactions on Robotics and Automation 13(5), 776–782 (1997)
5. De Santis, A., Siciliano, B., De Luca, A., Bicchi, A.: An atlas of physical human–robot interaction. Mechanism and Machine Theoryn 43, 2008 (2008)
6. Feil-Seifer, D., Mataric, J.: Defining socially assistive robotics. In: 9th International Conference on Rehabilitation Robotics. pp. 465–468. Chicago, IL, USA (2005)
7. Ficuciello, F., Villani, L., Siciliano, B.: Variable impedance control of redundant manipulators for intuitive human-robot physical interaction. IEEE Transactions on Robotics 31(4), 850–863 (2015)
8. Haddadin, S., aLBU Schäffer, A., Hirzinger, G.: Requirements for safe robots: Measurements, analysis and new insights. The International Journal of Robotics Research 28, 1507–1527 (2009)
9. Hogan, N.: Impedance control: An approach to manipulation: Parts I–III. ASME Journal of Dynamic Systems, Measurement, and Control 107(2), 1–24 (1985)
10. Huynh, D.: Metrics for 3D rotations: Comparison and analysis. Journal of Mathematical Imaging and Vision 35, 155–164 (2009)
11. Iggidr, A., Sallet, G.: On the stability of nonautonomous systems. Automatica 39, 167–171 (2003)
12. Khatib, O.: Inertial properties in robotic manipulation: An object-level framework. International Journal of Robotics Research 14(1), 19–36 (1995)
13. Maaroof, O.W., Dede, M.: Physical human-robot interaction: Increasing safety by robot arms posture optimization. In: Parenti-Castelli, V., Schiehlen, W. (eds.) ROMANSY 21-Robot Design, Dynamics and Control. CISM International Centre for Mechanical Sciences (Courses and Lectures), pp. 329–337. vol 569. Springer, Cham (2016)

14. Oh, Y. nad Chung, W., Youm, Y.: Extended impedance control of redundant manipulators based on weighted decomposition of joint space. Journal of Intelligent and Robotic Systems 15(5), 231–258 (1998)
15. Ott, C.: Control of nonprehensile manipulation. In: Cartesian impedance control of redundant and flexible joint robots, Springer Tracts in Advanced Robotics, vol. 49. Springer, New York, NY, USA (2008)
16. Ott, C., Kugi, A., Nakamura, Y.: Resolving the problem of non-integrability of null-space velocities for compliance control of redundant manipulators by using semi-definite lyapunov functions. In: 2008 IEEE International Conference on Robotics and Automation. pp. 1999–2004. Pasadena, CA, USA (2008)
17. Sadeghian, H., Villani, L., Keshmiri, M., Siciliano, B.: Multi-priority control in redundant robotic systems. In: 2011 IEEE/RSJ International Conference on Intelligent Robots and Systems. pp. 3752–3757. San Francisco, CA, USA (2011)
18. Sadeghian, H., Villani, L., Keshmiri, M., Siciliano, B.: Task-space control of robot manipulators with null-space compliance. IEEE Transactions on Robotics 30(2), 493–506 (2014)
19. Siciliano, B., Sciavicco, L., Villani, L., Oriolo, G.: Robotics: Modelling, Planning and Control. Springer, London, UK (2009)
20. Vigoriti, F., Ruggiero, F., Lippiello, V., Villani, L.: Control of redundant arms with null-space compliance and singularity-free orientation representation. Robotics and Autonomous Systems 100, 186–193 (2018)